ORIGINAL PAPER

Dynamic Behavior of Small Scale Nailed Soil Slopes

Debabrata Giri · Aniruddha Sengupta

Abstract The shaking table tests are conducted on small scale nailed embankment slopes to study their behavior under dynamic conditions. Medium grained local sand with a water content of 3% is used in the study. The embankment slope is constructed using the controlled-volume compaction method. Three slope angles, 30°, 35° and 40° with a constant slope height of 18 cm are considered for the embankment. Each slope is reinforced with six number of hollow aluminum nails in two rows. The ratio of the length of nail to slope height (0.82) is same for all model slopes. The nails are inserted at three different inclinations. Three strain gauges are glued to each nail to obtain local strains during shaking. The accelerations at the base and the crest of the model slopes are monitored to find the acceleration responses of the embankments during the input ground motions. The numerical simulation of the model tests is performed by a commercial program called FLAC. The results of the numerical analyses are found to be reasonably close to the corresponding experimental results.

List of symbols

c	Cohesion, kPa
c_c	Coefficient of curvature
c_u	Uniformity coefficient
D_r	Relative density
G	Shear modulus, kPa
G_{dyn}	Dynamic shear modulus, kPa
K	Bulk modulus, kPa
K_{bond}	Bond shear stiffness, kPa
ϕ	Angle of friction, degree
$\gamma_{d(max)}$	Maximum dry unit weight, kN/m^3
$\gamma_{d(min)}$	Minimum dry unit weight, kN/m^3
A	Cross-sectional area of nails, mm^2
ρ	Density of aluminum, kg/m^3
T_y	Yield strength
T_c	Compressive strength

D. Giri (✉)
Department of Civil Engineering, ITER,
Bhubaneswar, India
e-mail: debagiri@rediffmail.com

A. Sengupta
Department of Civil Engineering, IIT, Kharagpur, India

1 Introduction

The basic concept of soil nailing is to reinforce and strengthen the slopes and excavations by installing closely spaced steel bars called 'nails'. This process creates a reinforced section that by itself is stable and able to retain the ground around it. The soil–nail composition also increases apparent cohesion of the

soil through its ability to carry tensile loads. Soil nailing being an advanced area of research in Civil Engineering, literature study indicates a number of model and large field tests have been done by various researchers to understand the behavior of nailed slopes. Stocker et al. (1979) and Gassler and Gudehus (1981) conducted large-scale field tests on nearly vertical nailed cuts in cohesionless soil. Schlosser (1982) developed a multi-criteria based design method for nailed soil structures. Kitamura et al. (1988) and Gutierrez and Tatsuoka (1988) conducted a number of small-scale model tests of reinforced slopes and measured the tensile (reinforcement) forces and strain fields. Juran et al. (1988) used small-scale models to investigate the effect of construction method on the behavior of reinforced soil and nailed soil structures. Schlosser (1991) conducted a full-scale test on nailed soil wall leading it to fail progressively by saturating the reinforced soil mass. Pedley (1992) conducted long term tests on a 15 m high nailed wall in cohesive soil. Davis et al. (1993) investigated the behavior of steel reinforced slope by conducting a series of model tests in clayey sand.

The seismic performance of nailed soil structures is of great importance especially for the earthquake prone zones. The observations during the 1989 Loma Prieta Earthquake in the San Francisco Bay, where several nailed structures were subjected to significant levels of shaking (Barar et al. 1990) confirmed the need for a comprehensive investigation of the dynamic performances of nailed soil slopes. As nailed soil structures are coherent and flexible, they present inherent advantages of withstanding larger deformation with high resistance to dynamic loading. However, only limited studies are available to evaluate the dynamic responses of nailed soil slopes. Recently a small scale shaking table has been developed at IIT, Kharagpur completely indigenously to study the reinforced embankment slopes under cyclic conditions. This paper presents the development of the shaking table and the results of the tests performed to study the dynamic behavior of the reinforced embankment slopes. The surface displacements, settlement of the crest and the accelerations at the base and the crest of the slopes are measured during the tests. The effect of nail inclination and variation of induced nail force with respect to slope angle are also investigated. The tests are also simulated numerically using a finite element program called FLAC (Itasca Consulting

Group, Inc. 2005). The results of the numerical analyses are then compared with those obtained from the shaking table tests.

2 Development of the Shaking Table

A new shaking table experimental setup is developed at the Indian Institute of Technology, Kharagpur by using a 2,800 rpm and 7 HP DC motor. A slotted circular mild steel disc of 300 mm diameter and 20 mm thick is bolted to another circular disc of same size (used as a support to the slotted disc). The supported disc is connected to the shaft of the motor. A steel crank shaft 500 mm long, 20 mm in diameter is connected to the slotted disc by bolts. The other end of the crank shaft is connected to a reciprocating rod, 500 mm long and 20 mm in diameter. The amplitude of sinusoidal motion can be varied by changing the position of crank shaft in the calibrated slot of the disc. The other end of the reciprocating rod is connected to the shaking table's base plate. The reciprocating rod is kept in the horizontal position during motion by a bracket support. The speed of the motor can be controlled from a panel board which essentially consists of an electrical variant. A schematic diagram of the experimental set up is shown in Fig. 1. The newly developed shaking table has a maximum stroke length of 150 mm and a peak frequency of 50 Hz.

A system calibration has been done to check the performance of the experimental setup before starting the experimental work. The layout of the instruments for the calibration purpose is shown in Fig. 2a. The loading sequence used for the system calibration consists of a 10-s of horizontal sinusoidal motions with peak acceleration of 0.1 g at 4.65 Hz frequency and is shown in Fig. 2b. The responses of the two
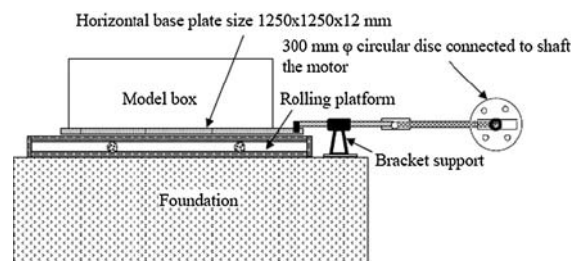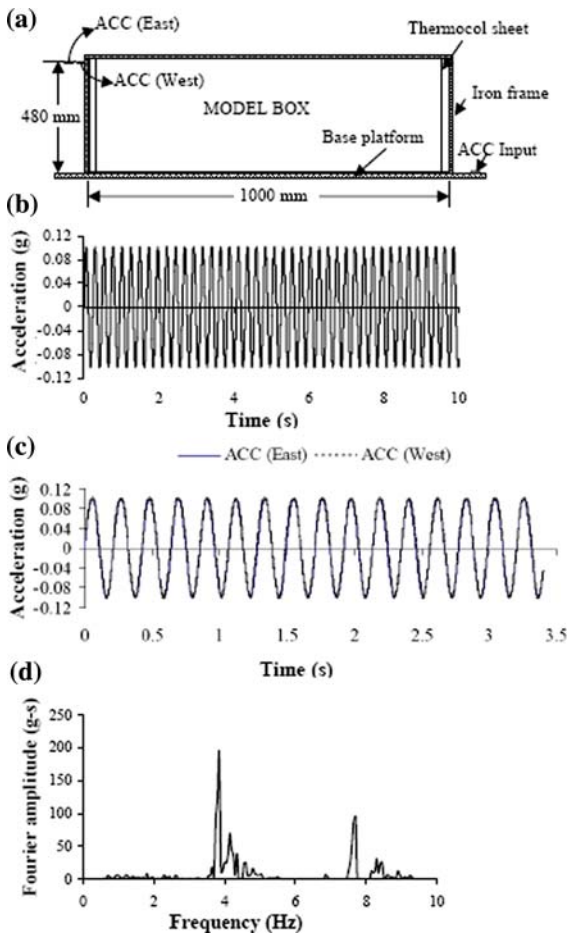

Fig. 1 A schematic diagram for experimental setup

Fig. 2 **a** Location of the accelerometers in the test setup; **b** input horizontal acceleration; **c** recorded horizontal acceler-ations in the box during calibration; **d** frequency content of the measured horizontal acceleration
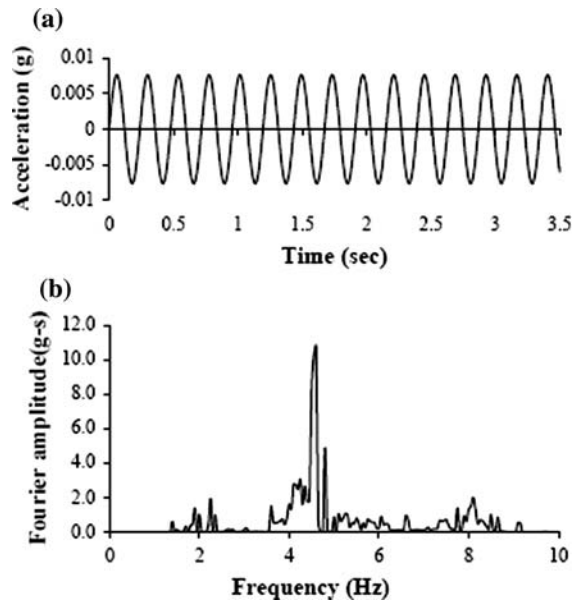

Fig. 3 **a** Measured vertical component of the acceleration during calibration; **b** frequency content of the vertical motion

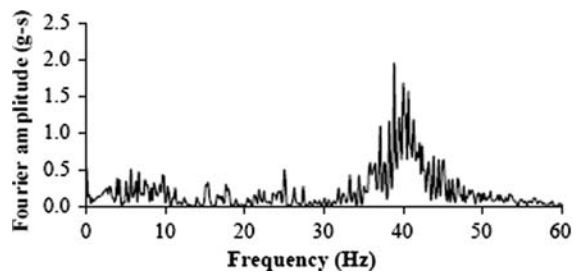Fig. 4 Frequency content of the whole test setup with soil slope

accelerometers fixed to the model box are shown in Fig. 2c. It is observed that no significant amplifica-tion of the system is registered during the loading and the system appears to behave linearly throughout the loading history. The responses of the accelerometers are found to be sinusoidal with predominant fre-quency of 4.65 Hz (see Fig. 2d). This corresponds to a payload of 2 kN (weight of the base plate and the empty model box). The vertical vibration of the shaking base plate and the model box is also measured and shown in Fig. 3. The magnitude of the vertical vibration (0.0075 g) of the base plate is very less as compare to the horizontal input motion and can not significantly affect the test results. The natural frequency of the base plate along with the test container and the soil slope is determined

experimentally by subjecting the whole test setup to a motion and then allowed it to shake freely until it stops by its own. As may be seen from the Fig. 4, the natural frequency of the whole test set up is much higher than the predominant frequency of the system given in Fig. 2.

3 Specimen Preparation and Material Properties

The soil used in this study is a local uniform medium sand (Kasai River sand). The grain size distribution of the sand is shown in Fig. 5. It is classified as poorly graded sand (SP), according to the Unified Soil Classification System. The specific gravity of the
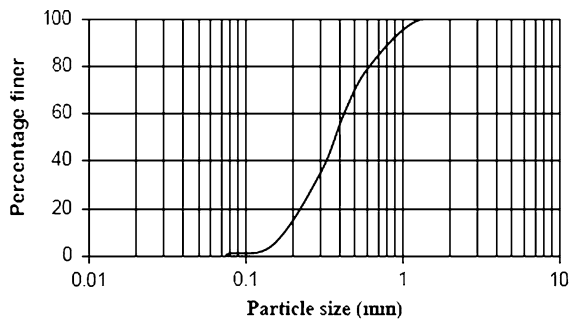
Fig. 5 Grain size distribution of the Kasai River sand used in the study

Table 1 Properties of the Kasai River sand and the aluminum nail

	Value
Soil property	
Unit weight γ at $D_r = 60\%$	15.02 kN/m³
Cohesion, c	1.0 kPa
Friction angle, ϕ	32°
Static shear modulus, G	3.61 MPa
Static young's modulus, E	9.528 MPa
Dynamic shear modulus, G_{dyn}	23.9 MPa
Dynamic bulk modulus, K_{dyn}	36.3 MPa
Reinforcement property	
Elastic modulus, E (at 2% strain)	134,800 GPa
Yield strength, T_y	5,640 N/m²
Compressive strength, T_c	0
Cross section area, A	201.1428 mm²
Shear bond stiffness, K_{bond}	4.215 MPa
Density, ρ	2,550 kg/m³

sand is 2.7. The maximum dry unit weight $\gamma_{d(max)}$ is 16.7 kN/m³, and the minimum dry unit weight $\gamma_{d(min)}$ is 14.03 kN/m³. The uniformity coefficient (c_u) and coefficient of curvature (c_c) of the sand are found to be 2.84 and 0.87, respectively. In all the model tests, the bulk unit weight of the sand is maintained at 15.02 kN/m³ and at a relative density, D_r of 60%. The drained triaxial shear test is performed on the soil sample to find its shear strength parameters. The cohesion and angle of friction are obtained from triaxial (drained) test as 1.0 kPa and 32°, respectively. The static Young's modulus (E) and static shear modulus (G) are computed from the initial portion of the stress–strain curves as 9.528 and 3.61 MPa, respectively assuming a Poisson's ratio of 0.3. The dynamic shear (G_{dyn}) and bulk (K_{dyn}) modulii for the sand are obtained from Baidya and Murali Krishna ([2001]) as 23.9 and 36.3 MPa, respectively assuming a Poisson's ratio of 0.3. These values were obtained indirectly from block vibration tests on the same sand. From the laboratory tests, elastic modulus hollow aluminum nails is found to be 135 GPa. The ultimate yield stress and ultimate load of a nail are obtained as 2,631 MPa and 61 kN, respectively. Table [1] shows all the strength parameters for the Kasai sand and the aluminum nails.

Before the construction of the model slopes, 3% water is added to the sand. The slope models are constructed in the test box by compacting the cured sand up to the desired height by controlled-volume method. The slope surface is prepared by a hand modeling tool. The 18-cm high slopes with slope angles 30°, 35° and 40° are considered here. Three numbers of aluminum hollow nails with constant vertical spacing of 6 cm is inserted into the model slopes in a single row. Two such rows of

reinforcements are used for each model slope. The spacing between the rows in horizontal directions is 0.27 m. Each hollow aluminum nail is 3 mm thick and 8 mm in outer diameter. Sand particles are glued to the outer surface of the nails to generate surface roughness. Three strain gauges of type BKCT-3 (resistance 119.2 ± 0.2 ohms, gauge factor: $1.92 \pm 2\%$ and gauge length 3 mm) are glued at equal spacing in each nail to record local shear strains. The hollow nails are used to conveniently route the cables from the strain gauges to the data acquisition system. The ratio of length of nail to slope height is kept same (=0.82) throughout this study. The nails are anchored at three different inclinations—horizontally, perpendicular to slope face and at 20° below the horizontal axis. A total number of nine reinforced model slopes are investigated.

4 Response of the Slopes

All the nine reinforced slopes are subjected to the same base acceleration which consists of sinusoidal motions with a constant peak acceleration of 0.1 g and frequency 4.65 Hz. Note that this is the same motion for which the test setup is calibrated before. The development of the sliding surface and the crest settlement are monitored with the progress of the
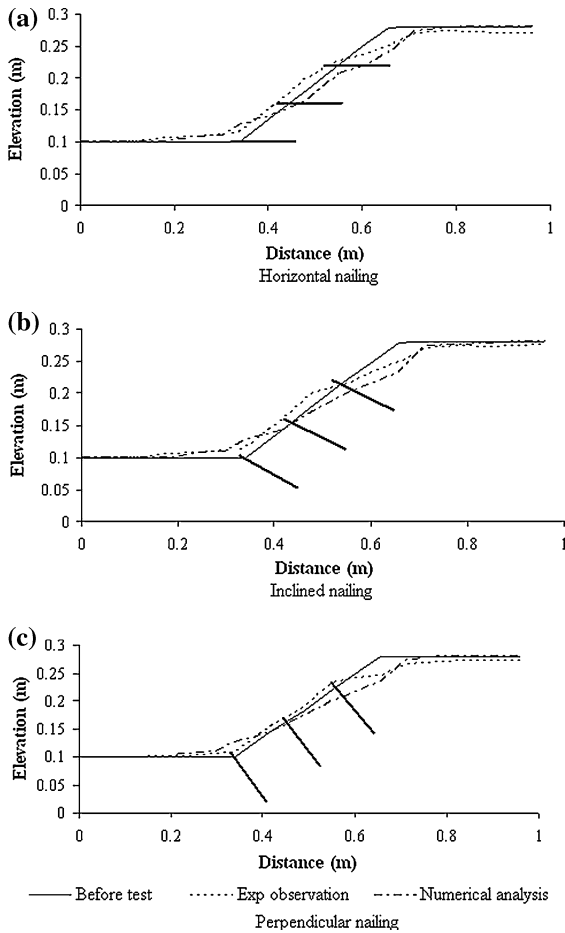
Fig. 6 Comparison of deformed slopes between experimental observations and numerical analyses for the 30° slope angle

Fig. 7 Comparison of deformed slopes between experimental observations and numerical analyses for the 35° slope angle

tests. The sliding surface and the crest settlement at the end of each test are shown in Figs. 6, 7 and 8. Figure 9 shows a side view of the 30° slope model depicting the slope failure observed at the end of a test. The side views for the other slopes are not shown to keep this paper brief. The results in general indicate that the development of the sliding surface and separation of the soil body near the crest is more prominent. The failure surface is developed near the mid width for all cases and appeared to be deeper for steep slopes, which is consistent with the field observations of earthquake induced landslides (Khazai and Sitar 2004). The experimental results show that the crest settlement is maximum (46 mm) for the 40° model slope when perpendicular nailing is used. A minimal settlement value of 25 mm is found for 30° model slope with horizontal nailing. In each
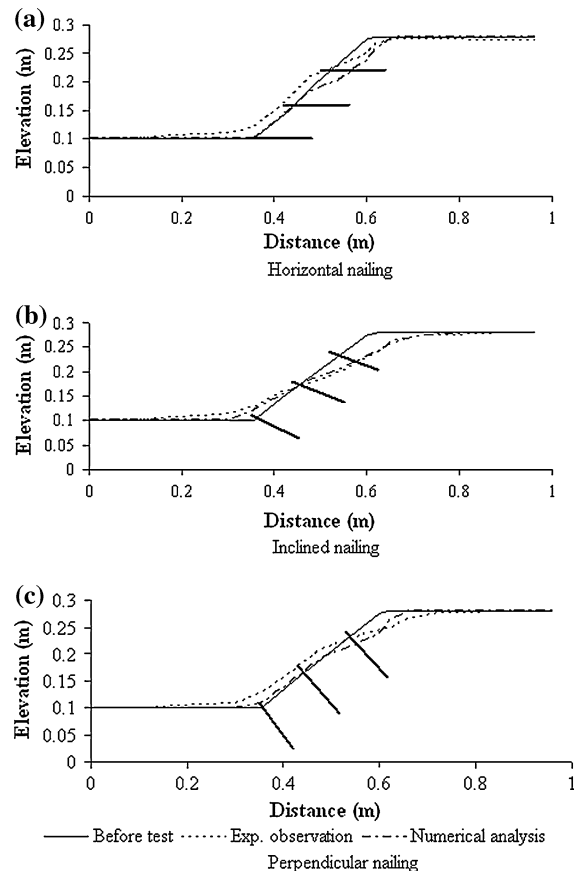
model slope, crest settlement is more when perpendicular nailing is used. In order to observe the effect of reinforcements, three 18 cm high, unreinforced model slopes at 30°, 35° and 40° slope angles were tested at the same loading conditions. These tests show maximum crest settlement of 55 mm for the 40° slope. The sliding surface and the crest settlement at the end of each test for these unreinforced model slopes are shown in Fig. 10. Table 2 shows a comparison of crest settlement obtained for the different cases. It is very clear that the crest settlement is reduced when slopes are reinforced. The failure surface close to the crest is more or less circular. Some hairline tension cracks at the crest are also prominent. These cracks are more prominent and more in numbers for the models with 30° slope angle. Less number of cracks is developed when the slope angle is more. This may be due to the fact that the slope becomes more unstable with the increase in
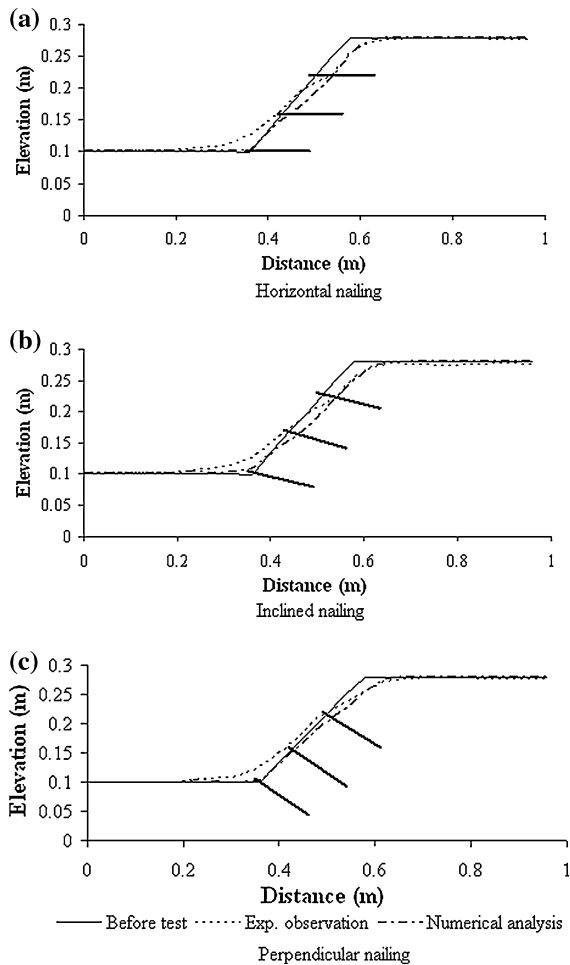
(a)

Horizontal nailing

(b)

Inclined nailing

(c)

——— Before test ········· Exp. observation – - – - Numerical analysis

Perpendicular nailing

Fig. 8 Comparison of deformed slopes between experimental observations and numerical analyses for the 40° slope angle

(a)

Failed side view of unreinforced slope.

(b)

Failed side view of reinforced slope.

Fig. 9 A typical deformed slope observed at the end of shaking table tests for the 30° slope cases

slope angle and the sliding (failure) surface is shallower as the slope fails at less number of loading cycles.

Four accelerometers are used to obtain acceleration responses during the tests. The positions of the accelerometers along with the locations of the nails with strain gauges in a schematic model slope are shown in Fig. 11a. Two accelerometers are attached to the shaking table base platform to get horizontal and vertical input acceleration parameters. Another two accelerometers are placed at the centre of base and crest of the soil slopes. The applied horizontal motions are same for all the cases and also essentially same as recorded by the accelerometer located at the base of the slope. The response (only the first 1-s of the motion) of the accelerometer at the base is shown
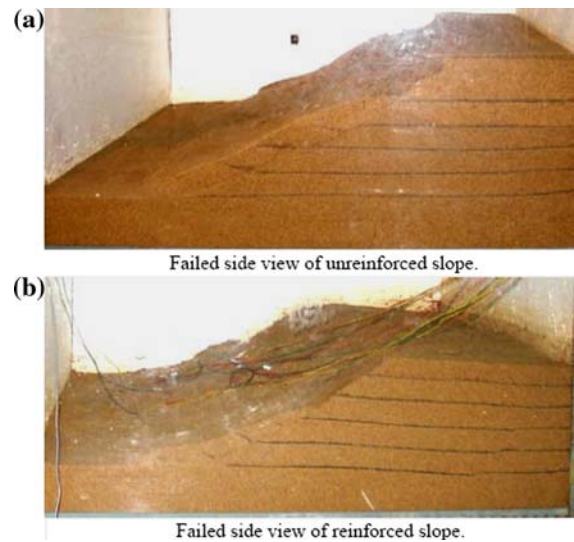
in Fig. 11b. The crest acceleration histories of all the slopes are recorded. Table 2 summarizes the magnification (ratio of the recorded crest acceleration and recorded base acceleration) of the acceleration through the slopes and the maximum crest settlement for each test. A minimal amplification factor of 1.006 is obtained for 30° model slope when reinforced with inclined nails. A maximum amplification factor of 1.065 is obtained for the 35° slope with perpendicular nailing.

Local strains in each nail are measured continuously at specified locations of each nail during the loading cycles. The reinforcement forces are calculated from the measured average strains using the load-strain relationship determined from the tensile test on aluminum nail specimen. The variation of reinforcement forces as deduced from the obtained strain gauge readings are shown in Figs. 12, 13 and 14. The figures show that the induced nail force varied nonlinearly with respect to loading time. An exception is noticed for the top nail which does not generate significant force as compare to other nails. This is likely due to the lack of adequate soil confinement at the shallow depth of soil cover. The induced reinforcement force for bottom layer of nails is maximum (249.24 N) for the 40° model slope when reinforced with inclined nails. A minimal value of 10.3 N for the top reinforcement layer is obtained for 30° model slope when perpendicular nailing is
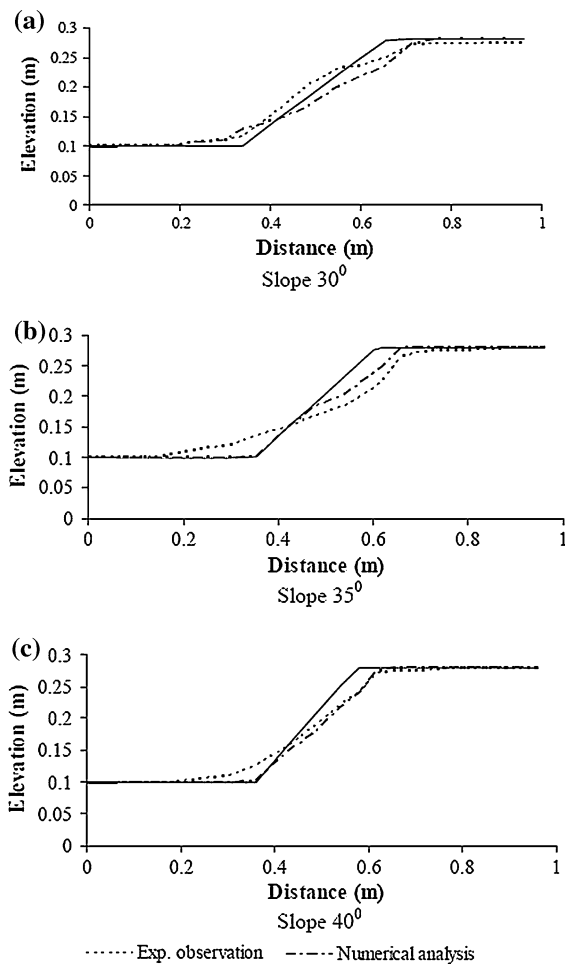
Fig. 10 Side view of failed unreinforced model slopes

used. It is observed that the reinforcement force is minimum for each model slope when perpendicular nailing is used. The induced reinforcement force for each model slope is summarized in Table 3. The side views of failed soil slopes as shown in Figs. 6, 7 and 8 indicate shallow failure surface even for the 40° slope angle when nails are anchored at right angle to the slope surface.

5 Numerical Analyses of the Model Slopes

A computer program FLAC developed by the Itasca Consulting Group (2005) is utilized for the dynamic analyses of the nine slopes studied. The FLAC has been successfully used in the past (Wang 2001; Wang

et al. 2004; Roth et al. 1993) for the dynamic analysis of soil embankments. The FLAC (Fast Lagrangian Analysis of Continua) computes stresses and strains in a continuum by a finite difference method. It uses an explicit solution method. The Lagrangian analysis allows for distortion of the grid so that the end state at each node is the beginning state of the next stress cycle. The soil is modeled as a material obeying the Mohr–Coulomb yield criteria. The nail reinforcements are modeled as cable elements. The bending effects are not important as the cable elements are sufficient to allow the modeling of a shearing resistance along their length. The bonding is provided by the shear resistance between the cable elements and the soil mass. The cable element formulation in FLAC considers more than just the local effect of the reinforcement. Its effect in resisting deformation is also accounted for along its entire length. The cable is assumed to be divided into a number of segments with nodal points located at each segment's ends. The mass of each segment is lumped at the nodal points, as in the continuum formulation of FLAC. The axial behavior of reinforcement systems may be assumed to be governed entirely by the reinforcing element itself. As the reinforcing element is slender, it offers very little bending resistance and can be treated as a one dimensional member with capacity to sustain uniaxial tension only. In the present analysis, the axial stiffness is described in terms of nail cross sectional area and Young's modulus, E. The aluminum nails are installed at a spacing of 0.27 m in the between them in the horizontal direction. This spacing is used by FLAC to scale the reinforcement properties and the actual cable forces in the cable elements. The shear bond stiffness, K_{bond}, for nail can be calculated from a numerical estimate of the elastic shear stress, τ_G, obtained from an equation describing the shear stress at the grout interface (St. John and Van Dillen 1983) given by

$$\tau_G = \frac{G}{\left(D/2 + t\right)} \frac{\nabla u}{\ln(1 + 2t/D)} \tag{1}$$

Where ∇u, is the relative displacement between the element and the surrounding material, G is the grout shear modulus, D is the reinforcement diameter and, t is the annulus thickness. However, FLAC also permits the following expression to provide a reasonable estimate of K_{bond}

Table 2 Comparison of the crest settlement and crest amplification between the shaking table experiments and the FLAC analyses

| Slope angle (°)	Maximum crest settlement (mm) without nailing Exp. result	Nail inclination	Experimental results	
			Maximum crest settlement (mm)	Amplification at the crest
30	28	Horizontal	25	1.027
		20°	26	1.006
		Perpendicular	33	1.032
35	50	Horizontal	31	1.009
		20°	39	1.042
		Perpendicular	41	1.065
40	55	Horizontal	26	1.042
		20°	37	1.023
		Perpendicular	46	1.052
Slope angle (°)	Maximum crest settlement (mm) without nailing Numerical result	Nail inclination	Numerical results	
			Maximum crest settlement (mm)	Amplification at the crest
30	42	Horizontal	24	1.010
		20°	28	1.004
		Perpendicular	36	1.023
35	40	Horizontal	29	1.00
		20°	40	1.038
		Perpendicular	38	1.056
40	49	Horizontal	25	1.036
		20°	36	1.018
		Perpendicular	44	1.043
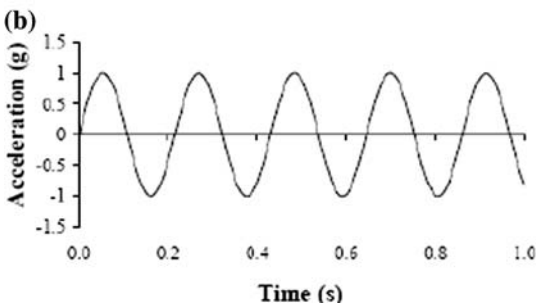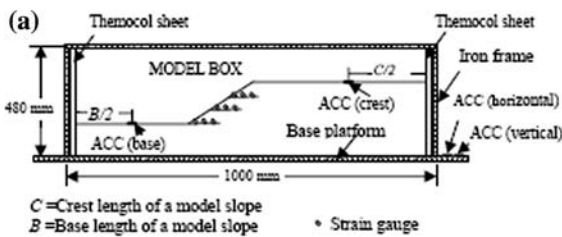
Fig. 11 **a** Location of the accelerometers, and strain gauges on nails anchored to the soil slope; **b** horizontal base acceleration measured during the tests

$$K_{\text{bond}} = \frac{2\pi G}{10 \ln\left(1 + \frac{2t}{D}\right)} \qquad (2)$$

The one-tenth factor in the above equation helps to account for the relative shear displacement that occurs between the nail and the actual borehole surface. This relative shear displacement (∇u) is not accounted for in the present formulation. The computed K_{bond} and other material properties of aluminum nail as obtained from the laboratory tests are tabulated in Table 1. The cohesion, c, friction angle, ϕ, unit weight, γ dynamic shear modulus, G_{dyn}, and dynamic bulk modulus K_{dyn} are specified for the soil. The soil parameters are based on the laboratory test results and are summarized in Table 1. In the numerical modeling, the container and the shaking table are not modeled. The soil slopes are discretized by quadrilateral elements. A typical discretization of the soil slope is shown in Fig. 15. The bottom of the
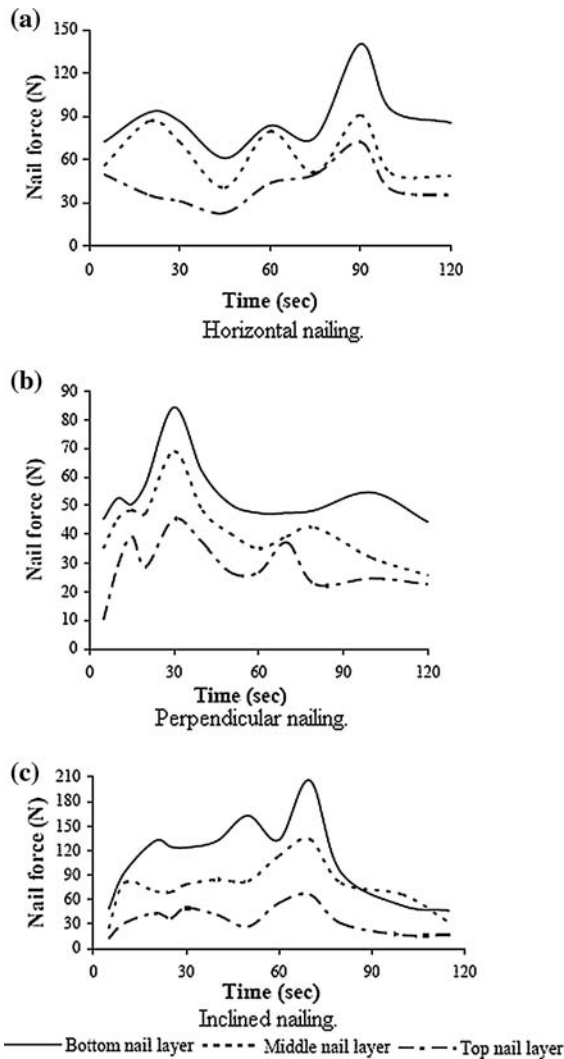
Fig. 12 Variation of nail force for the 30° slope angle

Fig. 13 Variation of nail force for the 35° slope angle

slopes is assumed to be fixed. The two side boundaries are assumed to be on roller (horizontal deformation is restricted). At the beginning, a gravity turn-on analysis is performed and the stresses are allowed to reach equilibrium state in static condition under self weight only. The dynamic analysis is then followed by prescribing the horizontal acceleration at the base of the model. This acceleration is the same sinusoidal motion recorded by the accelerometer pickups fixed to the shaking table and shown in Fig. 11b. The wave reflections at the two extreme side boundaries are minimized by specifying free field boundary conditions at those locations. The crest
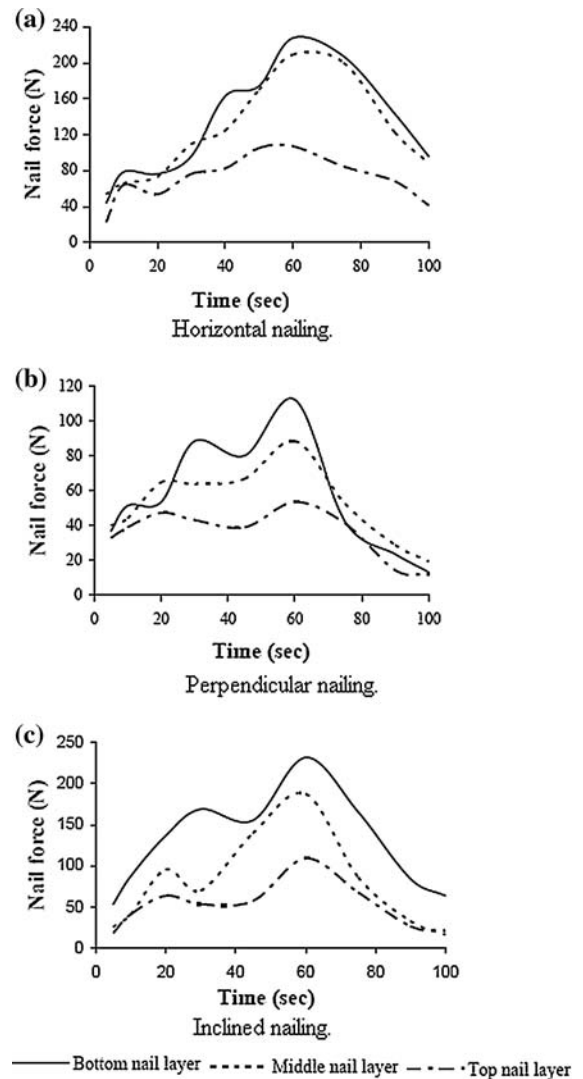
acceleration, and slope deformations are calculated with time. Figures 6, 7 and 8 show the numerical results in terms of displacement of the slopes at the end of the shaking and compare them with those observed in the laboratory shaking table tests. Numerical analysis predicts that the crest settlement is minimum (24 mm) for 30° model slope when horizontal nailing is used. A comparison of the maximum crest settlement for the model slopes with different nail configurations is presented in Fig. 16. A minimal amplification factor of 1.004 is obtained for the 30° model slope with inclined nailing. This finding is again consistent with the test results. The
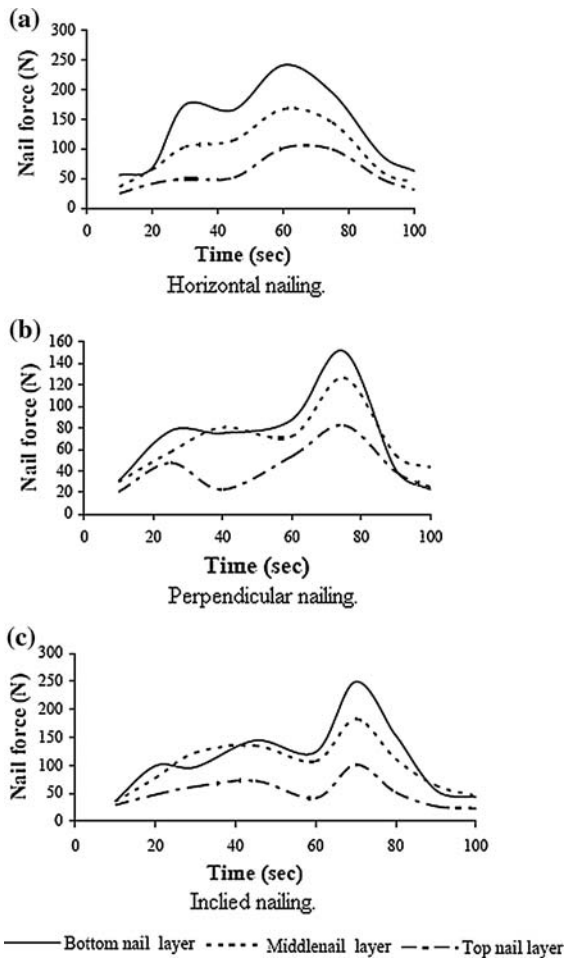
Fig. 14 Variation of nail force for the 40° slope angle

maximum crest settlement and the amplification of motion through the slopes are shown and compared with the corresponding test results in Table 2. The numerical model predicts softer responses for the 30°

and 35° slopes while for the 40° slope, the numerical analyses yield stiffer responses. Overall the numerical results are in reasonable agreements with the laboratory shaking table results.

6 Conclusions

A new shaking table is developed which is found to be performing well. The system calibration shows linear behavior during the tests. Nine reinforced soil slope models have been tested in the shaking table to study the effect of slope angle and nail inclination during cyclic loading. Based on these tests performed, the following conclusions are drawn:

1. The failure surfaces appeared to be shallow, likely to be circular and confined to the zone near the slope surfaces. These observations are consistent with the reported field observations of earthquake induced landslides.
2. The top view of failed slopes shows that numbers of major cracks along with some hairline cracks developed near the box boundary walls. These hairline cracks may be due to the boundary wall confinement and do not interfere with the development of the major failure surface. However these cracks disappear as the slope angle increased.
3. Some intermediate cracks are also developed near the boundary and between major failure surfaces. It is likely that more than one set of failure surfaces might have developed during the laboratory shaking table tests.
4. Number of cracks appeared to be less as the slope angle increases. With the increase in

Slope angle (°)	Nail inclination	Maximum reinforcement force (N)		
		Top nail	Middle nail	Bottom nail
30	Horizontal	72.09	90.63	140.08
	20°	65.92	133.89	205.98
	Perpendicular	45.32	69.00	84.45
35	Horizontal	107.11	209.07	227.64
	20°	109.17	187.45	231.74
	Perpendicular	53.56	88.57	112.26
40	Horizontal	100.95	166.85	241.04
	20°	102.0	192.30	249.24
	Perpendicular	82.42	126.75	151.45

Table 3 Comparison of reinforcement forces

Fig. 15 Numerical discretization of a reinforced soil slope

■ Horizontal nailing ▲ Inclined nailing ● Perpendicular nailing

——— Numerical analysis ------- Exp. observation
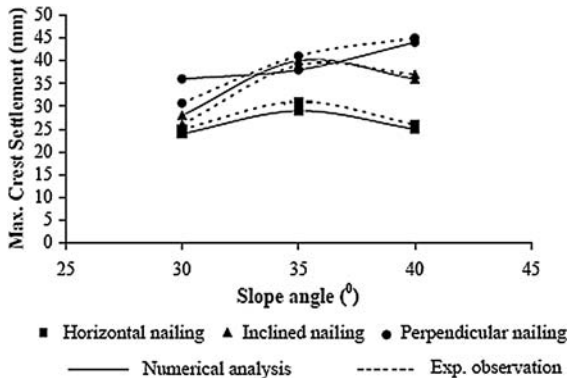
Fig. 16 A comparison of the maximum crest settlement for the model slopes with different nail configurations

slope angle, the slope becomes more unstable and fails with less number of loading cycles. The mass movement and size of possible failure wedge decrease with decrease in loading cycles. This may be the reason for the development of less number of failure cracks in steep slopes.

5. The magnitude of base acceleration for all model slopes is almost same as the applied input acceleration. The base slope height is same for all model slopes and base slope failure does not occur during shaking.

6. The induced nail force varied nonlinearly with respect to loading cycles and the top nail does not generate significant force as compared to other nails. This is likely due to the lack of adequate soil confinement.

7. The magnitude of induced nail force increases as the steepness of slope increases. This may be the reason why with the increase in slope angle, the mass of the failure wedge is more. The magnitude of nail force is minimal when nails are anchored at perpendicular to the slope surface.

8. The magnification between the amplitude of crest acceleration for moderate steep slope (30° and 35°) is more. With the increase in slope

steepness, the magnitude of crest acceleration decreases.

9. The numerical analyses adequately reproduced the response of the model slopes in the frequency and the time domains. A close match is found for the acceleration responses with the experimental test results.

10. The slope and crest displacements computed by the FLAC are found to be reasonably close to those observed in the shaking table tests.

References

Baidya DK, Murali Krishna G (2001) Investigation of resonant frequency and amplitude of vibrating footing resting on a layered soil system. Geotech Test J (ASTM) 24(4):409–417

Barar O, Felio GY, Vucetic M, Chapman R (1990) Performance of soil nailed walls during the October, 17, 1989, Loma Prieta earthquake. In: Proceedings of forty-third Canadian Geotechnical Conference, Quebec, pp 165–173

Davis MCR, Jacob CD, Bridle RJ (1993) An experimental investigation of soil nailing retaining structures. Thomas Telford, London

Gassler G, Gudehus G (1981) Soil-nailing: some aspects of a new technique. In: Proceedings of the Tenth ICSMFE, Stockholm, pp 665–670

Gutierrez V, Tatsuoka AF (1988) Role of facing in reinforcing cohesionless soil slopes by means of metal strips. In: Proceedings of the international geotechnical symposium on theory and practice of earth reinforcement, Kyushu, Japan, pp 289–294

Itasca Consulting Group, Inc. FLAC Version 5 (2005) Fast lagrangian analysis of continua: theory and background. Itasca Consulting Group, Minneapolis

Juran I, Guermazi A, Chen CL, Ider MH (1988) Modeling and simulation of load transfer in reinforced soil. Int J Numer Anal Methods Geomech 12:141–155

Khazai B, Sitar N (2004) Evaluation of factors controlling earthquake induced landslides caused by Chi-Chi earthquake and comparison with the Northridge and Loma Prieta events. Eng Geol 71(1):79–95

Kitamura T, Nagao A, Uehara S (1988) Model loading tests of reinforced slope with steel bars. In: Proceedings of the international geotechnical symposium on theory and practice of earth reinforcements. Kyushu, Japan, pp 311–316

Pedley MJ (1992) Ground modification on soil and rock anchorage, rock bolting, soil nailing and dowelling. Soil Nailing Lecture Notes on Ground Modification Seminar, University of Technology, Sydney, pp 51–89

Roth WH, Inel S, Davis C, Brodt G (1993) Upper San Fernando Dam 1971 revisited. In: Darnton DW, Plathby SC (eds) Annual Conference Proceedings of the Association of State Dam Safety Officials, Lexington, Kentucky, pp 49–60

Schlosser F (1982) Behavior and design of soil nailing. In: Proceedings of the symposium on recent developments in ground improvement techniques. Bangkok, pp 399–413

Schlosser F (1991) Discussion: the multi-criteria theory in soil nailing. Ground Eng Nov:30–33

St. John CM, Van Dillen DE (1983) Rock bolts: a new numerical representation and its application in tunnel design in rock mechanics—theory-experiment-practice. In: Proceedings of the 24th US symposium on rock mechanics, Texas A&M University, pp 13–26

Stocker MF, Korber GW, Gassler G, Gudehus G (1979) Soil nailing. In: Proceedings of the International Conference on Soil Reinforcement. Paris, pp 469–474

Wang ZL (2001) Simulation of earthquake performance of a waterfront slope using fully coupled effective stress approach. FLAC and numerical modeling in Geomechanics. In: Proceedings of the 2nd International FLAC Conference, Lyon, France, pp 101–108

Wang ZL, Makdisi FI, Egan J (2004) Practical applications of a nonlinear approach to analysis of earthquake-induced liquefaction and deformation of earth structures. In: Proceedings of the 11th International Conference on Soil Dynamics & Earthquake Engineering, University of California, Berkeley, pp 299–306